# A parameterization of Greenland's tip jets suitable for ocean or coupled climate models

David A. J. Sproson,[1] Ian A. Renfrew,[1] and Karen J. Heywood[1]

Received 25 November 2009; revised 5 March 2010; accepted 24 March 2010; published 20 August 2010.

[1] Greenland's tip jets are low-level, high wind speed jets forced by an interaction of the synoptic-scale atmospheric flow and the steep, high orography of Greenland. These jets are thought to play an important role in both preconditioning for, and triggering of, open-ocean convection in the Irminger Sea. However, the relatively small spatial scale of the jets prevents their accurate representation in the relatively low resolution (~1 degree) atmospheric (re-)analyses which are typically used to force ocean general circulation models (e.g. ECMWF ERA-40 and NCEP reanalyses, or products based on these). Here we present a method of 'bogussing' Greenland's tip jets into such surface wind fields and thus, via bulk flux formulae, into the air-sea turbulent flux fields. In this way the full impact of these mesoscale tip jets can be incorporated in any ocean general circulation model of sufficient resolution. The tip jet parameterization is relatively simple, making use of observed linear gradients in wind speed along and across the jet, but is shown to be accurate to a few m $s^{-1}$ on average. The inclusion of tip jets results in a large local increase in both the heat and momentum fluxes. When applied to a 1-dimensional mixed-layer model this results in a deepening of the winter mixed-layer of over 300 m. The parameterization scheme only requires 10 meter wind speed and mean sea level pressure as input fields; thus it is also suitable for incorporation into a coupled atmosphere-ocean climate model at the coupling stage.

**Citation:** Sproson, D. A. J., I. A. Renfrew, and K. J. Heywood (2010), A parameterization of Greenland's tip jets suitable for ocean or coupled climate models, *J. Geophys. Res.*, *115*, C08022, doi:10.1029/2009JC006002.

## 1. Introduction

[2] Greenland, with its steep, high orography, presents a significant barrier to atmospheric flow, and is well situated to interact with synoptic-scale weather systems moving along the North Atlantic storm track. This interaction can lead to a local acceleration of low-level winds. Barrier winds form where relatively stable air is advected toward Greenland and is unable to pass over the plateau, and so-called 'tip jets' form at the southernmost point of Greenland, Cape Farewell, as air is deflected over or around the cape by a nearby cyclone [*Doyle and Shapiro*, 1999; *Moore and Renfrew*, 2005]. These jets can be westerly (forward), associated with a parent cyclone between Greenland and Iceland, or easterly (reverse), associated with a cyclone to the south of Cape Farewell (Figure 1). These localized winds can be very intense: scatterometer measurements have suggested 10-meter wind speeds of up to 50 m $s^{-1}$ [*Moore and Renfrew*, 2005; *Renfrew et al.*, 2008], and direct observations have confirmed 10-meter winds of over 30 m $s^{-1}$ [*Renfrew et al.*, 2009b]. Such winds occurring anywhere could be expected to have a profound effect on the ocean below, however this is especially true in the sub-polar seas where the ocean may become sufficiently preconditioned for deep convective overturning to occur [*Marshall and Schott*, 1999].

[3] Oceanic convection has long been known to take place in the central Labrador Sea [*Wüst*, 1935], where a closed cyclonic gyre provides ideal preconditioning and cold-air outbreaks from the North American continent can rapidly remove large quantities of heat from the ocean. The deepest mode water formed here, Labrador Seawater (LSW), forms an important part of the Atlantic meridional overturning circulation (MOC) [*Talley and McCartney*, 1982]. In contrast to the Labrador Sea, the Irminger Sea, the basin to the east of Greenland south of the Denmark Strait, has received little attention as a possible site of oceanic convection, despite early evidence that deep mixed layers did indeed occur here [*Nansen*, 1912]. This is largely due to the fact that the Irminger Sea was not considered to be appropriately preconditioned, and the atmospheric forcing in the area was not considered to be strong enough to trigger convective overturning. In recent years, however, these ideas have been thrown into doubt. Observations of mid-depth float velocities have shown that there is a suitably strong recirculation present in the Irminger Sea sufficient to allow the ocean to become preconditioned for overturning [*Lavender et al.*, 2000], its largely barotropic nature having prevented the structure from being observed in hydrographic sections [*Pickart et al.*, 2003a]. These, combined with the very high wind speeds

[1]School of Environmental Sciences, University of East Anglia, Norwich, UK.


0148-0227/10/2009JC006002

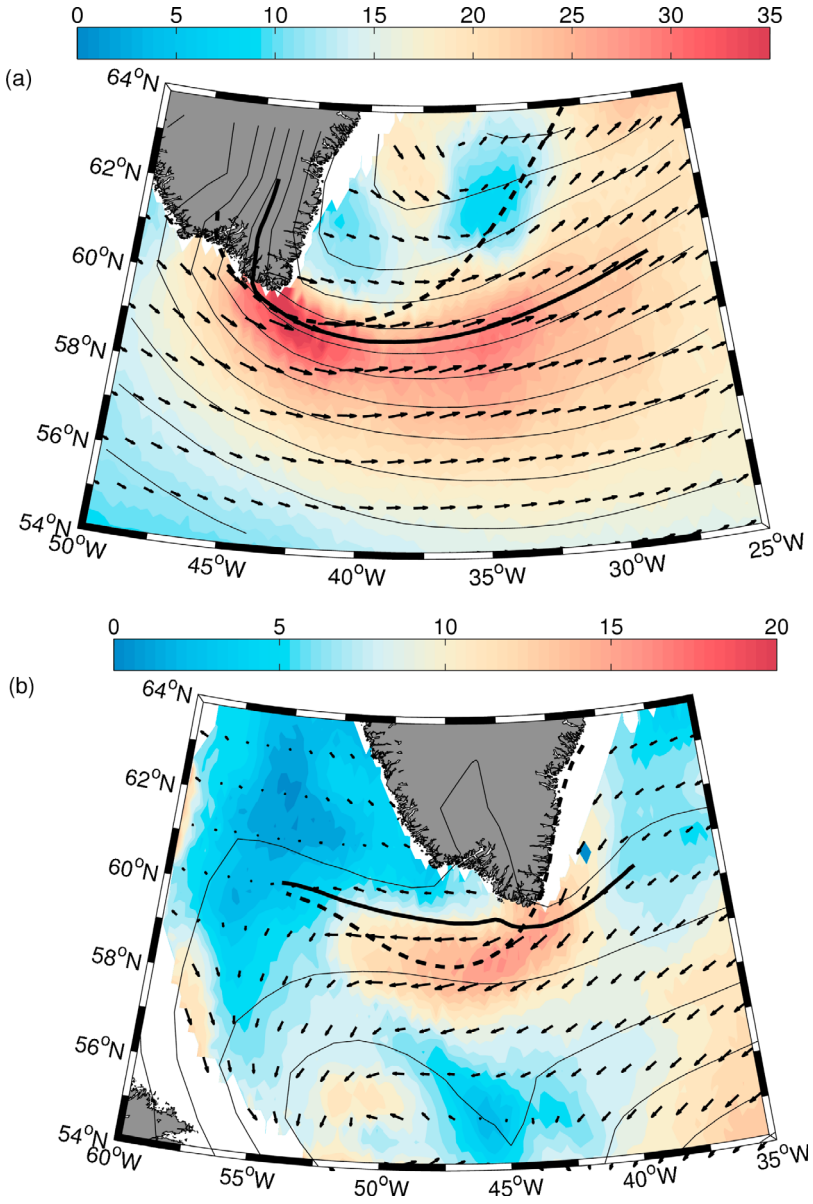


**Figure 1.** QuikSCAT wind speeds (shaded, m $s^{-1}$) and vectors (every 1 degree) showing typical (a) westerly and (b) easterly tip jets. Mean sea level pressure from ECMWF is contoured every 4 hPa. The overlaid lines show the paths where the core of parameterized tip jets would be placed using the geostrophic winds (solid) or 10 meter winds (dashed) as a guide.

associated with the tip jets, thought to result in heat fluxes locally exceeding 800 W $m^{-2}$ [*Doyle and Shapiro*, 1999], have forced the Irminger Sea to be reconsidered as a potentially important site for open ocean convection [*Pickart et al.*, 2003a]. This case has been strengthened through both one-dimensional [*Våge et al.*, 2008] and highly idealized three-dimensional [*Pickart et al.*, 2003b] modeling studies which have shown mixed-layers in the Irminger Sea with depths comparable to those observed in the Labrador Sea during active convection [*Pickart et al.*, 2002].

[4] Studying the impact of the tip jets in the framework of a global ocean general circulation model (OGCM), however, remains difficult as the relatively small scale of the tip jets results in their inadequate representation in the atmospheric models which are used to provide boundary conditions for OGCMs [*Renfrew et al.*, 2009a]. Simple linear relationships have been seen between the maximum wind speeds in the ECMWF ERA-40 reanalysis and scatterometer-observed winds during tip jet conditions [*Våge et al.*, 2009]. However, such simple scalings are not sufficient to improve the representation of the tip jet in OGCMs. They can only tighten spatial gradients that are already present, rather than introducing more realistic gradients in the wind speed. They also lead to an over-estimation of wind speeds away from the center of the jet. In this paper we present a more sophisticated method of parameterizing Greenland tip jets into the wind fields of atmospheric reanalyses which, when combined with bulk heat flux calculations, allows the full impact of these jets to be seen in OGCMs.

[5] The parameterization is used to 'bogus' in tip jets to the atmospheric wind fields (following operational forecasting terminology). The approach is somewhat similar to that of *Condron et al.* [2008], who bogussed polar mesoscale cyclones into atmospheric forcing fields, making use of a satellite-derived cyclone database, and then used these modified fields to force an ocean model. One advantage of our approach is that no such external data set is required; the parameterization is based solely on the near-surface wind and mean sea level pressure fields. Note that *Hu and Meehl* [2009] have recently used such a methodology to study the role of hurricanes on the Atlantic meridional overturning circulation.

[6] In the following two sections we describe the creation of a QuikSCAT-based data set which is then used to develop a simplified spatial description of tip jets. In section 4 we describe how this can be introduced into an ocean or coupled model to improve the representation of tip jets. Section 5 discusses the improvements in the distribution of wind speeds around Greenland, and Section 6 describes the impact the increased extreme wind speeds have on the air/sea fluxes over the Irminger and Labrador Seas. Finally, in Section 7 we use a 1-dimensional ocean mixed-layer model [*Price et al.*, 1986], used in previous studies of the impact of Greenland tip jets on the ocean [*Våge et al.*, 2008; *Sproson et al.*, 2008], to provide an example of the impact that the parameterized tip jets have on the development of the winter mixed-layer in the Irminger Sea. Conclusions of the study are given in Section 8.

## 2. Data Sets

[7] In order to create a data set of tip jets for use in the development of the parameterization, the archive of QuikSCAT passes from 1999 to 2007 was manually searched to identify passes in which a well-defined tip jet was present. QuikSCAT winds are available twice daily on a 0.25° grid (L3 gridded product), and are thus able to represent the strong wind speeds and spatial gradients associated with tip jets. If a tip jet was present in consecutive passes these were assumed to be the same jet, and only one of these passes was selected. The selected pass was that which occurred in the middle of the series. These remaining passes were then subjectively filtered to select only those which have a clear and distinctive tip jet, with little noise in the background wind field. The resulting data set consists of 32 well-defined westerly and 42 well-defined easterly tip jets. The data set spans all types of jet, from weak summer jets with peak winds less than 15 m $s^{-1}$, to robust winter jets with peak winds of over 35 m $s^{-1}$. Zonal extents range from approximately 100 km to over 1000 km.

[8] Using this data set, tip jets were isolated using a semi-objective method, whereby any point **p** on the QuikSCAT grid was considered to be part of the jet if $s_{\mathbf{p}} \geq \gamma s_{\max}$, where $s_{\max}$ is the maximum wind speed associated with the jet, $s_{\mathbf{p}}$ is the wind speed at **p**, and $\gamma \in (0, 1)$ is a threshold value used to delineate the jet from the background wind field. Additionally, **p** must be connected to the point of maximum wind speed by other grid points with a wind speed greater than or equal to that at **p**. This method is only semi-objective as, due to differing background wind fields, the value of $\gamma$ had to be chosen for each case to successfully isolate the jet from the background field. The value of $\gamma$ was chosen (subjectively) so that the edge of the jet was as close as possible to the point where the ECMWF analysis no longer substantially underestimated the wind speed in comparison with QuikSCAT. The value of $\gamma$ over our data set is fairly consistent, with a mean of 0.76 and standard deviation of 0.09. It is worth noting that although the subsequent parameterization is dependent on this value of $\gamma$ and on the cases in the data set, the number of cases is large enough to ensure that case-to-case variability does not lead to biases in the parameterization. This is discussed further later.

## 3. Spatial Description of a Tip Jet

### 3.1. Scaling the Jets

[9] Once the tip jets have been isolated from the background wind field, we study the spatial structure associated with the jets. In each case, the spatial evolution of wind speeds along the central axis of the jet and perpendicular to this axis at 25%, 50% and 75% of the distance along the central axis are extracted. Three examples of each of these are shown in Figure 2, with a linear least squares fit overlaid. In these three cases the gradients both along and across the jet are approximately linear, with a strong correlation between wind speed and distance either along or across the jet. This pattern is seen generally in the 32 westerly and 42 easterly tip jet test cases. Over these test cases, the Pearson correlation coefficients between wind speed and distance along the jet axis both have means greater than 0.7, statistically significant above the 94% level (Table 1).

[10] A total of 96 across-jet sections were taken from the 32 westerly tip jet test cases and 126 from the 42 easterly test cases. Again the decrease in wind speed can be well represented with simple linear gradients. There is, however, a small asymmetry between the gradients on the poleward and equator-ward sides of the jets (Figures 2d–2f), and so these cases are treated separately. The Pearson correlation coefficients between wind speed and distance from the jet axes have mean values greater then 0.95, statistically significant above the 94% level (Table 1). Therefore, we can, to a reasonable approximation, describe the spatial structure of both the westerly and easterly tip jets by a linear decrease in wind speed along and across the core axis of the jet from an assumed maximum wind speed. Determining the maximum wind speed will be discussed shortly.

[11] While the gradients along and across the jet are, in general, approximately linear, there are differences in these linear gradients from jet to jet. The range of these gradients along the jet and to the north/south of the jet for both the westerly and easterly jets is shown in Figure 3. These gradients may be thought of as free or 'tunable' variables for the parameterization, dependent on the metric used to describe the error in the parameterization. The approach we take here is to choose gradients which produce the best composite jet over all of our test cases while still maintaining an accurate characterization of individual jets. The best composites are found by searching over $0.002 \leq g_l \leq 0.031$, $0.001 \leq g_n, g_s \leq 0.21$, where $g_l$ is the along-jet gradient and $g_n$ and $g_s$ are the north and south across-jet gradients, respectively (all m $s^{-1}$ $km^{-1}$), and finding those where the 10, 15 and 20 m $s^{-1}$ isotachs most closely mirror those of the QuikSCAT composite. The gradients chosen are 0.014 m $s^{-1}$ $km^{-1}$ along the jet and 0.08 m $s^{-1}$ $km^{-1}$ and 0.05 m $s^{-1}$ $km^{-1}$ to the north and south of the jet respectively in the case of the westerly tip jet, and 0.016 m $s^{-1}$ $km^{-1}$ along the jet and 0.08 m $s^{-1}$ $km^{-1}$ and

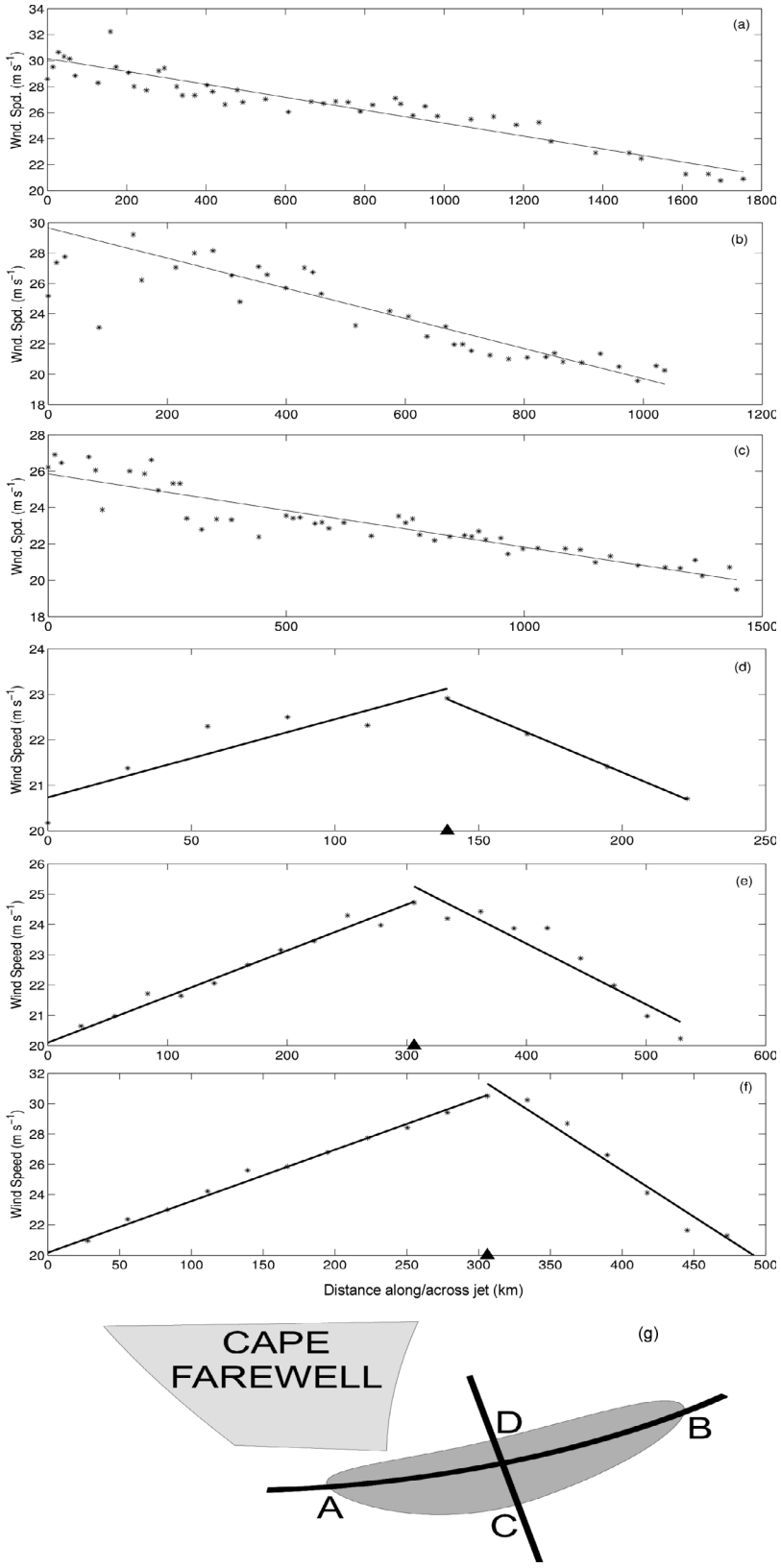


**Figure 2.** Examples of the decrease of wind speed from Cape Farewell (a–c) along the center of a tip-jet, line segment AB, and (d–f) across the jet at its midpoint, line segment CD. In Figures 2d–2f the center of the jet is highlighted with an arrowhead; to the left of this is the south flank of the jet and to the right is the north flank of the jet. The QuikSCAT winds are shown by the black stars, with a linear least squares fit overlaid. (g) A cartoon showing where gradients were taken from is given.

**Table 1.** Maximum, Minimum, Mean and Standard Deviation of the $r$ Values of the Linear Fits to the Decrease in Wind Speed Along and Across the Jets and the Mean Significance Level of These Fits

| | Max($r$) | Min($r$) | Mean($r$) | SD($r$) | Mean($P$) |
|---|---|---|---|---|---|
| Westerly along-jet | 0.96 | 0.56 | 0.86 | 0.10 | 99% |
| Easterly along-jet | 0.95 | 0.16 | 0.79 | 0.17 | 97% |
| Westerly across-jet (N) | 1.00 | 0.70 | 0.96 | 0.06 | 94% |
| Westerly across-jet (S) | 1.00 | 0.75 | 0.96 | 0.05 | 96% |
| Easterly across-jet (N) | 1.00 | 0.04 | 0.95 | 0.11 | 94% |
| Easterly across-jet (S) | 1.00 | 0.15 | 0.95 | 0.12 | 94% |

0.05 m $s^{-1}$ $km^{-1}$ to the north and south of the jet respectively in the case of the easterly tip jet. These are generally slightly higher than the mean and median observed gradients (see Figure 3), but are very close to these values and well within the range of gradients determined.

### 3.2. Placing the Jets

[12] One of the challenges of parameterizing the Greenland tip jet is the variation in character; no two tip jets are ever exactly the same in size, orientation or maximum wind speed. We thus need a robust technique for placing and scaling each jet based on the large-scale synoptic situation, which is in general skillfully reproduced in the atmospheric (re)analyses.

[13] Both the westerly and easterly jets, to a good approximation, originate at the tip of Cape Farewell [*Moore and Renfrew*, 2005]. The tip of Cape Farewell can thus be considered to be the start of the jets regardless of the synoptic situation. The jet then evolves downstream in approximate accordance with the surface wind field although, due to the surface drag re-orienting the surface wind vectors toward the parent low pressure center, this is not exact – rather the wind vectors are oriented to the left of the axis of the jet (Figure 1).

[14] *Våge et al.* [2009] noted that, in a climatological sense, the westerly jet is a surface extension of the upper-level jet stream, which thus acts partly to steer the jet. The upper level jet is high enough to be almost completely unaffected by drag imposed at the surface and is thus very well approximated by the geostrophic relationship $\mathbf{v_g} = \frac{\hat{\mathbf{k}}}{f} \times \nabla_p \Phi$, where $\mathbf{v}_g$ is the horizontal geostrophic velocity, $f$ is the Coriolis parameter, $\Phi$ is the geopotential and $\hat{\mathbf{k}}$ is a unit vector in the vertical. Consequently, it may be expected that the path of the westerly jet axis may be better related to the mean sea level geostrophic wind than the 10-meter wind, and this is indeed seen to be the

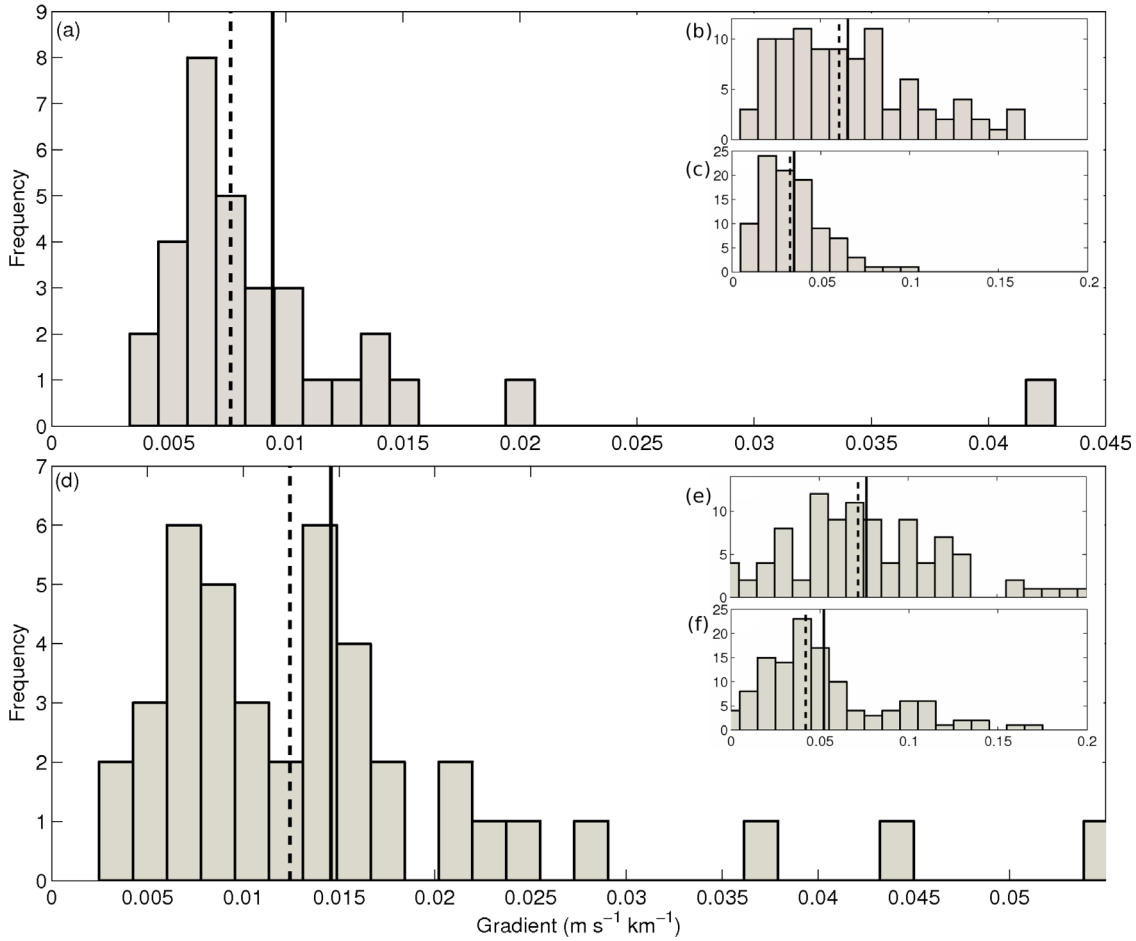


**Figure 3.** Distribution of wind speed gradients for the westerly and easterly tip jets from our QuikSCAT data set, as illustrated in Figure 2. (a) Along the center of the westerly jet; (b) across the north flank of the westerly jet; (c) across the south flank of the westerly jet; (d) along the center of the easterly jet; (e) across the north flank of the easterly jet; (f) across the south flank of the easterly jet. Solid and dashed lines show the mean and median respectively.

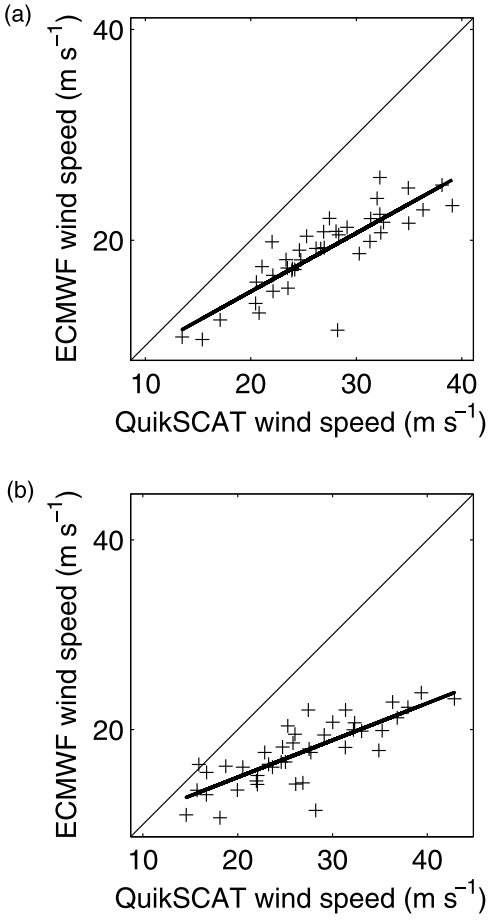


**Figure 4.** Scatterplot showing the relationship between the maximum wind speed in QuikSCAT and in ECMWF in the areas (a) 56–60 °N, 36–44 °W, and (b) 56–62 °N, 40–54 °W, where westerly and easterly tip-jets respectively occur most commonly. A linear least squares fit is overlaid in each case.

case. Figure 1a shows a path generated using the 10-meter geostrophic wind which closely matches the path of a westerly tip jet observed by QuikSCAT. We therefore use the mean sea level geostrophic wind in the parameterization to determine the path for the westerly tip jet.

[15] In general, easterly tip jets evolve from barrier flows along the south-east coast of Greenland [*Moore*, 2003; *Moore and Renfrew*, 2005; *Outten et al.*, 2009]. Such flows have a strong ageostrophic component (i.e. the vector difference between the true wind and the geostrophic wind) and thus a path cannot be created using the geostrophic winds. Instead we must resort to using the 10 meter wind field to create a path for the jet. The easterly tip jet can thus be oriented slightly too far to the south, however this is to a much lesser degree than the westerly tip jet would be displaced to the north were the 10 meter wind field to be used to generate its path. Figure 1b shows a path generated using the 10-meter wind which closely matches the path of a easterly tip jet observed by QuikSCAT.

### 3.3. Peak Wind Speed

[16] Here we use the ECMWF operational data set, at ECMWF ERA-40 resolution, henceforth ECMWF, as a 'proxy' for the ECMWF ERA-40 reanalysis (henceforth ERA-40), which has too little temporal overlap with QuikSCAT. The ERA-40 reanalysis is of relatively high resolution (T159 ~ 1.125°) for a global reanalysis, and performs well in comparison to the NCEP/NCAR reanalysis in the sub-polar regions [*Renfrew et al.*, 2002, 2009a]. The ERA-40 reanalysis does contain a representation of the Greenland tip jet, albeit one that is spatially too smooth and significantly too weak in magnitude [*Våge et al.*, 2009]. A comparison of the maximum wind speed in ECMWF with that in QuikSCAT for our 32 westerly test cases, over the area 56–60 °N, 36–44 °W, where tip jets are most likely to be observed [*Moore and Renfrew*, 2005], reveals that ECMWF underestimates the peak wind in a very linear fashion (Figure 4). Thus a least squares linear fit provides a simple model to estimate the maximum wind speed in a westerly tip jet from the corresponding wind field in ECMWF:

$$S_{\text{tipjet}} = \frac{S_{\text{ECMWF}} - 6.241}{0.493}, \tag{1}$$

where $S_{\text{tipjet}}$ is the maximum wind speed in the tip jet parameterization, and $S_{\text{ECMWF}}$ the maximum wind speed in ECMWF.

[17] *Ebuchi et al.* [2002] noted that there is a possibility that QuikSCAT becomes slightly biased high at particularly high wind speeds. This cannot be clearly seen in Figure 4, and the removal of the five data points with the highest wind speeds has a negligible effect on the relationship. Despite this, implementation of this regression may result in excessively strong peak winds on the rare occasions that the wind speeds in ECMWF are sufficiently strong (greater than around 24 m s$^{-1}$ for the westerly tip jet or 21 m s$^{-1}$ for the easterly tip jet). To prevent this happening, we limit the maximum wind speed of the bogussed tip jet to 35 m s$^{-1}$, a value which has been seen at the surface in high resolution mesoscale simulations of the Greenland tip jet [*Doyle and Shapiro*, 1999; *Outten et al.*, 2009; C. Hay et al., A case study of a Greenland lee cyclogenesis event and the subsequent spawning of a tip jet, manuscript in preparation], and observed near the surface [*Renfrew et al.*, 2009b]. This gives us, for the westerly tip jet, the relationship

$$S_{\text{tipjet}} = \begin{cases} \frac{S_{\text{ECMWF}} - 6.241}{0.493} & \text{if } S_{\text{ECMWF}} < 23.496, \\ 35 & \text{otherwise.} \end{cases} \tag{2}$$

[18] Proceeding similarly, the maximum speed in an easterly tip jet may be given by the relationship

$$S_{\text{tipjet}} = \begin{cases} \frac{S_{\text{ECMWF}} - 7.159}{0.391} & \text{if } S_{\text{ECMWF}} < 20.84, \\ 35 & \text{otherwise,} \end{cases} \tag{3}$$

over the area given by 56–62 °N, 40–54 °N.

### 3.4. Temperature and Humidity

[19] Although wind speed is an important factor in setting the strength of the air-sea heat and momentum exchange, the vertical gradients of both humidity and temperature also play important roles. Figure 5 shows composites of 2 meter temperature and specific humidity for the 32 westerly tip jets (Figures 5a and 5b) and 42 easterly tip jets (Figures 5c and 5d) on which the parameterization is based. The composites are

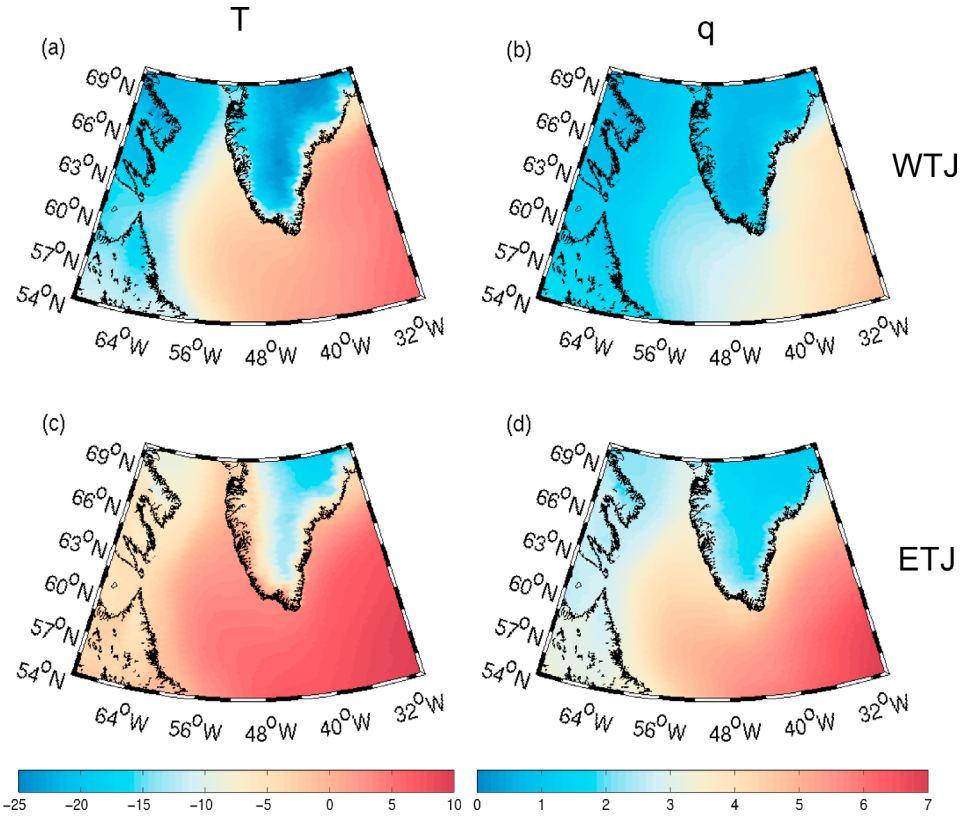


**Figure 5.** Composites of (a, c) 2 meter temperature (°C) and (b, d) specific humidity (g kg$^{-1}$) for all of the 32 westerly (Figures 5a and 5b) and 42 easterly (Figures 5c and 5d) tip jet cases used in this study, from the North American Regional Reanalysis (NARR).

from the North American Regional Reanalysis (NARR) data set [*Mesinger et al.*, 2006], which has a 32 km horizontal resolution. In the westerly case, the area around Cape Farewell is relatively cold and dry, with average temperatures of around 0 °C and specific humidities of around 2.5 g kg$^{-1}$. However, these values are simply due to the prevailing synoptic conditions; there are no mesoscale features evident in Figure 5. Any such mesoscale features should be resolved in the relatively high resolution NARR data set [*Renfrew et al.*, 2009a], however they would be sub-grid scale and therefore would not be consistently represented in the ECMWF reanalysis. Similarly, for the easterly tip jet (Figures 5c and 5d), although humidities and temperatures are generally higher than in the westerly case, no mesoscale features are apparent. Figure 5 suggests that it is not of first order importance to include temperature or humidity changes in the development of the tip jet parameterization and therefore we do not consider this any further.

## 4. Bogussing Technique

[20] The first consideration is *when* the parameterization should be called to place a tip jet into the wind field. There are fairly well-defined synoptic conditions that are observed to give rise to tip jets [*Moore and Renfrew*, 2005]. For example, both phenomena are tied to parent cyclones, between Greenland and Iceland in the case of the westerly tip jet and to the south of Greenland in the case of the easterly tip jet. However, while these large-scale situations may be necessary for the jets to exist, they are by no means sufficient and it would be very difficult to derive a robust method for calling the parameterization based on large-scale features in the mean sea level pressure field. During their construction of a QuikSCAT climatology of tip jets, *Moore and Renfrew* [2005] noted that the directions of strong winds around Cape Farewell were largely bimodal, with the vast majority coming from the west or north-east. These strong winds are closely associated with the (westerly and easterly, respectively) tip jets. We therefore assume that any strong wind from the west is associated with a westerly tip jet and any strong wind from the north-east or east is associated with an easterly tip jet.

[21] As illustrated via a flowchart in Figure 6, the algorithm proceeds as follows: first, the 10 m wind speed ($u_{10}$) immediately to the south of Cape Farewell is calculated. If this is found to be less than 10 m s$^{-1}$ (the approximate wind speed at which equations (2) and (3) start to cause an increase in the wind speed) then it is assumed that no tip jet is present and the parameterization routine stops. If the wind speed is greater than 10 m s$^{-1}$ then, depending on the sign of $u_{10}$ at Cape Farewell, a maximum perturbation wind speed is calculated for the westerly or easterly tip jet (equation (2) or (3)). If this is found to be less than 10 m s$^{-1}$ then again the routine stops. In the case of the easterly tip jet, a final check is carried out, ensuring that the parameterization is only called if the wind direction immediately to the south of Cape Farewell is between

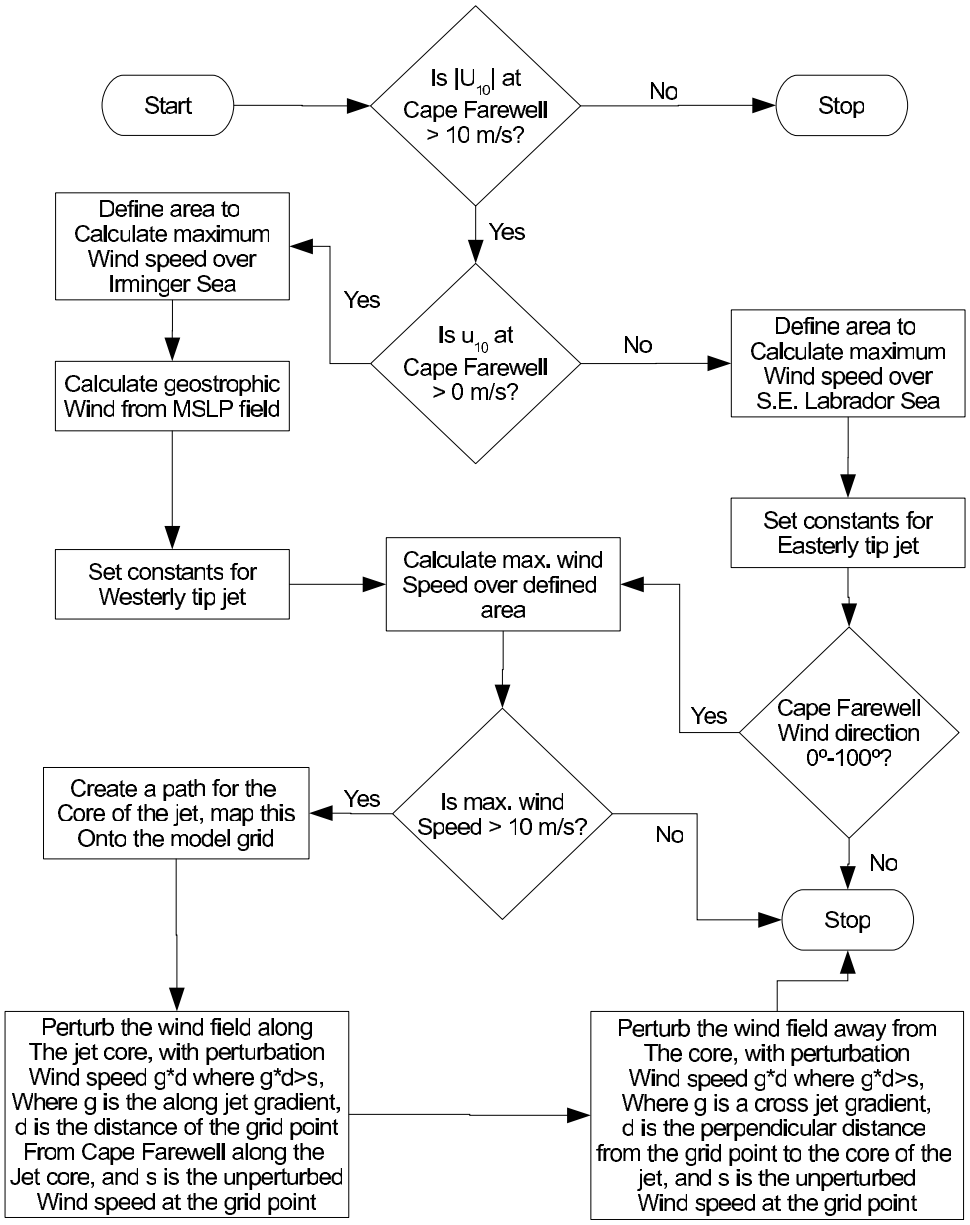


**Figure 6.** A flowchart describing the basic steps involved in inserting easterly and westerly tip jets into the wind field of an ocean model.

0° and 100°. This prevents invoking the parameterization in the case of any barrier type enhancement on the south-west coast of Greenland.

[22] Figure 7 shows, in schematic form, how the tip jet parameterization is implemented. Once it has been established that the parameterization needs to be invoked, the $u_g$ and $v_g$ components of the geostrophic wind (in the case of the westerly tip jet) are calculated from the mean sea level pressure field, which must be included as part of the atmospheric forcing data set. A point particle is then initialized just off the coast of Cape Farewell, at the climatological wind speed maximum of *Moore and Renfrew* [2005]. This maximum is around 15 m $s^{-1}$ in the DJF mean, however it is its presence rather than its magnitude which is important here. This particle is then advected into Greenland by $-(u_g, v_g)$ for the westerly tip jet, or by $-(u_{10}, v_{10})$ for the easterly tip jet and away from Greenland by $(u_g, v_g)$ for the westerly tip jet, or by $(u_{10}, v_{10})$ for the easterly tip jet, thus creating a path for the core of the tip jet. The exact length of this path will be dependent on the strength of $(u_g, v_g)$ or $(u_{10}, v_{10})$, however it is advected for long enough to exceed the extent of the tip jet for that wind speed (recall that this is linearly dependent on the maximum wind speed in the jet). This path, which is generated on the rational plane, is then mapped onto the model grid using a simple nearest neighbor technique. Once the path is on the model grid, the wind speed at the point nearest the climatological maximum wind speed is perturbed according to equation (2) or (3) as appropriate, and then the wind speed at each subsequent grid point along the path is perturbed by a slightly lesser amount, according to the model along-jet

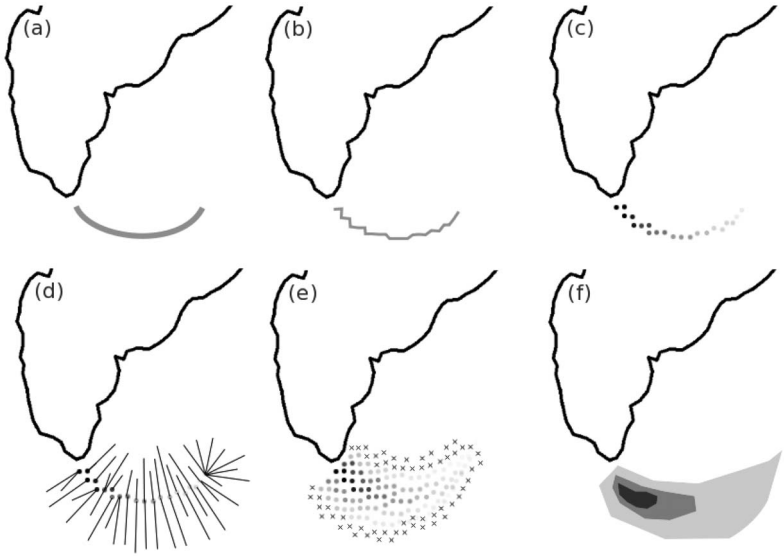


**Figure 7.** A schematic showing how tip jets are bogussed into the wind speed field. (a) A point is advected from near Cape Farewell by the geostrophic winds calculated from the mean sea level pressure field, thereby creating a path for the tip jet. (b) This path is then discretized onto the ocean model grid. (c) The wind field along the path is perturbed, starting from the maximum wind speed calculated via equation (2) and decreasing linearly until this speed would be less than the background wind field. (d) Grid points 'suitably' near the path are mapped onto it in as perpendicular a fashion as is possible. (e) Points away from the central path are perturbed by a factor inversely proportional to their distance from it, as long as this results in a wind speed increase; otherwise they are left unperturbed (crosses). (f) The bogussed tip jet.

gradient described earlier. This process ceases once the perturbation to the next grid point in the sequence would result in a wind speed value less than that of the background wind field. Once this is complete, we have a representation of the core of the jet bogussed into the wind field, and all that remains is to 'flesh out' the jet. In order to achieve this, all of the grid points in a domain covering the Irminger and Labrador Seas are surjectively mapped onto the core of the jet, with the mapping simply defined by minimizing the distance between each grid point and the core of the jet. This mapping ensures that the line connecting each point in the domain to that in the image is as perpendicular as possible, given the discrete nature of the model grid. Each of these grid points is then adjusted to the strength of the wind at the point on the jet core onto which it is mapped, multiplied by the distance between these two points and the appropriate across-jet gradient, if and only if the resulting speed is stronger than the unperturbed wind speed at that grid point.

[23] In Figure 8 a practical example of the parameterization scheme 'in action' is given. In the unperturbed ECMWF wind speed field there is a representation of the jet, however the very strong winds in the core of the jet are not represented and the peak wind speeds are only around 20 m $s^{-1}$ (Figure 8a). Figure 8b shows the wind speed field with just the core of the jet, which lies approximately along a line of constant mean sea level pressure, perturbed. Figure 8c shows the complete parameterized jet; peak wind speeds in the core of the jet are now up to around 28 m $s^{-1}$ and there is a relatively large area with wind speeds greater than 20 m $s^{-1}$. Note that the increased spatial gradients will also lead to an increase in wind stress curl on the flanks of the jet. Figure 8d shows the corresponding tip jet from the nearest QuikSCAT pass to this time. The location of the parameterized jet is not perfect when compared with QuikSCAT, however the spatial extent and the maximum in wind speed are very well reproduced. Note that while the core winds of the parameterized tip jet shown in Figure 8 are misplaced slightly to the south of the jet seen in QuikSCAT, this error is not a systematic feature of the parameterization scheme in the case of the westerly jet. Interpolating the ECMWF and ECMWF+TJ winds (Figures 8a and 8c) onto the QuikSCAT grid (Figure 8d) and then summing over all of the grid points where QuikSCAT data are non-NaN provides a method of quantifying the improvement in the wind field around Cape Farewell. This summation over the QuikSCAT data yields a value of 50127 m $s^{-1}$, while over the ECMWF data it yields only 36534 m $s^{-1}$. The perturbed wind field, ECMWF+TJ, sums to 46879 m $s^{-1}$, significantly closer to the QuikSCAT value than to the ECMWF value.

[24] Figure 9 shows composites of the entire data sets used to develop the westerly tip jet (32 cases) and the easterly tip jet (42 cases) parameterizations: for the ECMWF data, ECMWF with the parameterization and QuikSCAT. The composites here are relevant as the impact of a single tip jet on the ocean is likely to be small, but the integrated effect of tip jets over an entire winter may be climatologically important, for example in forcing convection in the Irminger Sea. In the westerly tip jet case, the composite parameterization is very well co-located with the composite QuikSCAT jet and compares very well in terms of wind speed magnitude. The easterly tip jet composite compares well in terms of wind speed magnitude, however it is not perfectly co-located with the easterly

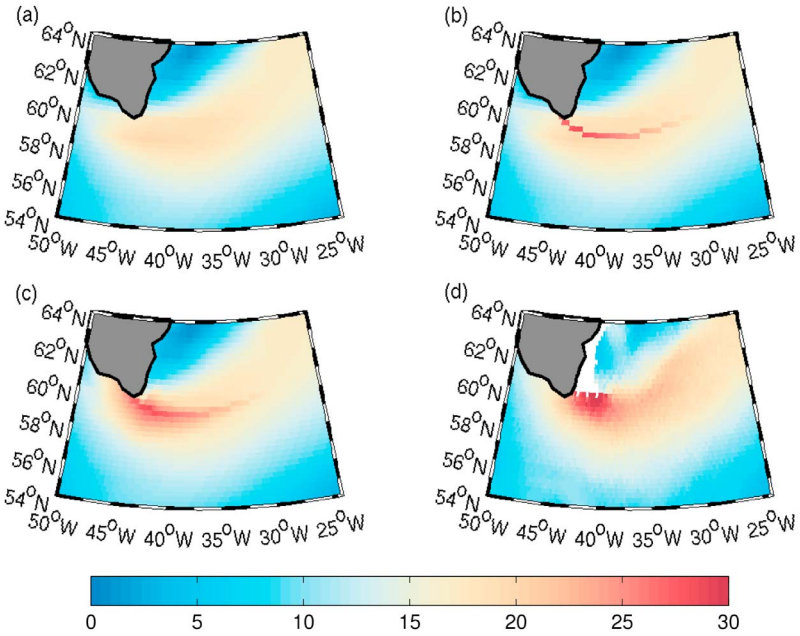


**Figure 8.** A practical example of the tip-jet bogussing algorithm. (a) The ECMWF wind speed field around Cape Farewell, interpolated onto a $\frac{1}{4}^{\circ}$ resolution grid. (b) The core of the jet laid out on the $\frac{1}{4}^{\circ}$ grid. (c) The bogussed tip-jet. (d) The corresponding tip-jet from the nearest QuikSCAT pass.

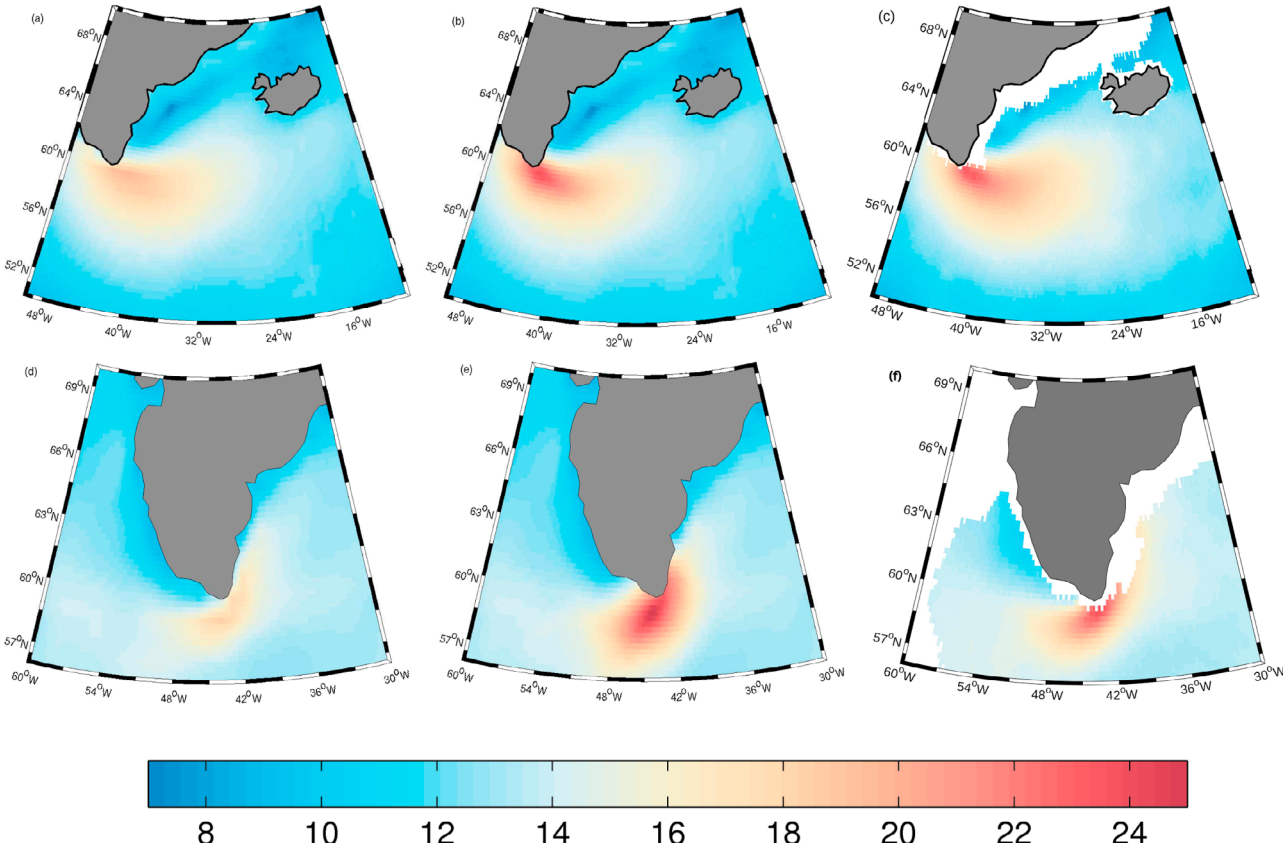


**Figure 9.** A composite of wind speed (colored, m $s^{-1}$) during the Greenland (a–c) westerly tip jet and (d–f) easterly tip jet for all of the cases used in the current study for ECMWF (Figures 9a and 9d), ECMWF with parameterization (Figures 9b and 9e) and QuikSCAT (Figures 9c and 9f). White areas show where no QuikSCAT data were available due to the presence of sea-ice or consistent heavy rainfall.

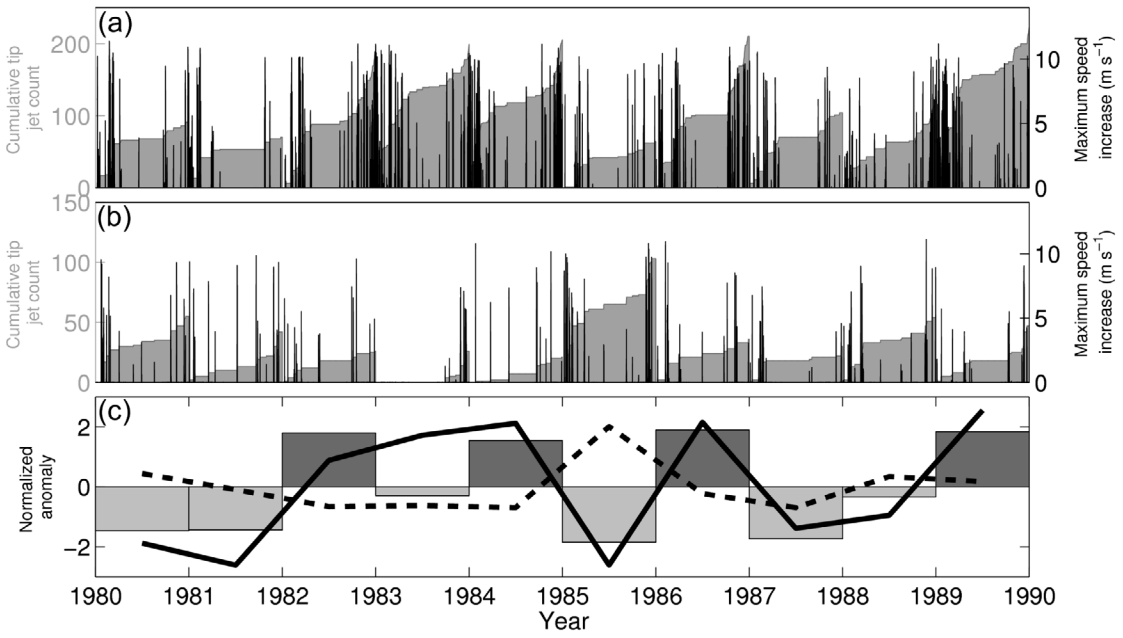


**Figure 10.** A representation of the tip jet parameterization between 1980 and 1990. The light gray shading shows the cumulative tip jet count for each year, and the black lines show the maximum wind speed difference between the parameterization and control for each tip jet. (a) Westerly tip jets and (b) easterly tip jets. (c) The NAO index (bars), calculated from ERA-40, together with a normalized tip jet occurrence anomaly for westerly tip jets (solid line) and easterly tip jets (dotted line).

jet in QuikSCAT, but has a slightly stronger meridional component. It is possible that this slight error could be minimized with the use of some nudging, however the methodology of such a technique is likely to be dependent on the nature of the model grid. As this is intended as a generic concept paper, we do not include such a technique. Figure 9 illustrates that, on average, the westerly and easterly tip jet parameterizations work well and are very realistic compared to satellite-derived winds.

[25] The number of occurrences of the westerly and easterly tip jet parameterization in the ERA-40 from 1980 to 1990, are related to the North Atlantic Oscillation, calculated from the mean sea level pressure difference between the Icelandic Low and the Azores High in the ERA-40 mean sea level pressure (Figure 10). The relative occurrences of the tip jets are shown as normalized anomalies compared with the 1980–1990 mean. The occurrence of the westerly tip jet is very well reproduced, with nearly all of the tip jets occurring in the winter, and a strong correlation between the number of tip jets in a year and the sign of the NAO, in agreement with previous studies of the Greenland tip jet [*Moore*, 2003; *Moore and Renfrew*, 2005; *Bakalian et al.*, 2007; *Våge et al.*, 2009]. The number of westerly tip jets parameterized is slightly larger than the number calculated by *Moore* [2003], who observed westerly tip jets occurring between 5% and 14% of the time, depending on the winter. The easterly tip jet is also slightly over represented compared to the climatology of *Moore* [2003], who saw the easterly tip jet occurring between 6% and 12% of the time during the winter, depending on the phase and strength of the NAO. The difference is largely because we are considering a tip jet to occur whenever the parameterization is called, whereas *Moore* [2003] only considered events with wind speeds greater than gale force (17 m s$^{-1}$). In cases where the wind is less than gale force, the parameterization is called, but will result in only small perturbations to the ERA-40 wind field. Counting a tip jet to occur every time the wind field is perturbed over this period, approximately 3000 westerly and 2000 easterly tip jets are seen to occur, corresponding to 750 and 500 tip jet days respectively.

## 5. Wind Speed Distributions

[26] A successful method of describing the distribution of the winds over the ocean is to use a two-parameter Weibull model [*Pavia and O'Brien*, 1986]. The Weibull distribution for a random variable $V$, with parameters $A$ and $C$, is given by

$$f(V;A,C) = \left[\left(\frac{C}{A}\right)\left(\frac{V}{A}\right)^{C-1}\right] e^{\left(\frac{V}{A}\right)^{C}}, \qquad (4)$$

where $A$ (m s$^{-1}$) is a scaling parameter and $C$ is a dimensionless shape parameter. Figure 11 shows Weibull distributions and illustrates that both the ECMWF wind speed distribution and the ECMWF+TJ parameterization wind speed distribution are biased low when compared with the QuikSCAT distribution. This is to be expected given the systematic differences between ECMWF and QuikSCAT at high wind speeds seen in previous studies [*Ebuchi et al.*, 2002; *Renfrew et al.*, 2009a]. The inclusion of a mesoscale feature such as a tip jet cannot be expected to remedy this systematic bias, however it should improve the wind speed distribution. This is indeed the case, with the shape of the distribution in the parameterized wind field more closely

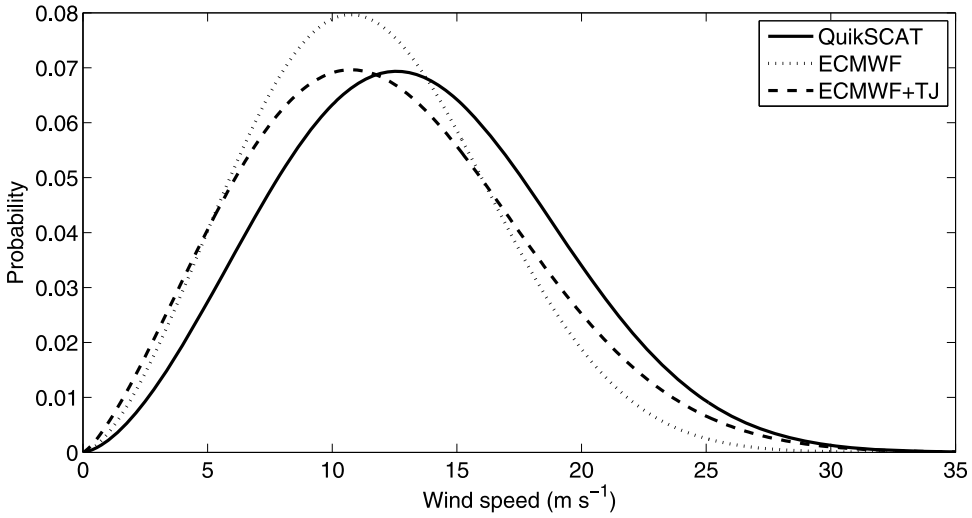


**Figure 11.** Weibull distributions of wind speed in the box given by 55–65 °N, 20–45 °W for QuikSCAT, ECMWF and ECMWF with tip jet parameterization over the 32 test cases.

resembling that of QuikSCAT, giving an increased probability of observing wind speeds in excess of 17 m s$^{-1}$.

[27] Improvements in the wind speed distribution can also be seen in simple statistics (Table 2). The changes caused by the parameterization are all consistent with an improved representation of the tip jet: the maximum wind speed has increased by over 9 m s$^{-1}$, with the mean wind speed increased by only around 0.6 m s$^{-1}$ because the increased wind speeds are limited to a small area. The minimum wind speed seen in ECMWF is unchanged. Arguably the most important statistic here is the standard deviation, giving a measure of the variability of the wind. If the parameterization is behaving appropriately then the standard deviation should be similar in the ECMWF+TJ and QuikSCAT winds, as the tip jet accounts for much of the variability in wind speed in this area [*Moore and Renfrew*, 2005]. Standard deviations of QuikSCAT and the ECMWF+TJ wind fields are 5.5 m s$^{-1}$ and 5.47 m s$^{-1}$ respectively, while that of the unperturbed ECMWF wind field is 4.8 m s$^{-1}$, indicating that the inclusion of the tip jet does improve the spatial variability of the wind with respect to the best observations available.

[28] *Chelton et al.* [2006] note that, in comparison with QuikSCAT, the surface wind fields in atmospheric (re)analyses lack power at high wave numbers. For spatial scales that are comparable to the model resolution, this is to be expected, however significant differences were seen at scales much larger than this, which the higher resolution models should be capable of resolving. Is it possible that some of this 'missing' variability is due to an under-representation in the models of mesoscale features such as tip jets? Figure 12 shows power spectral density over the 32 westerly tip jet cases over the north-east Atlantic (note that the upturned tail of the QuikSCAT curve is erroneous, and is due to the gridding and/or smoothing of the QuikSCAT data). Power should continue decreasing approximately with $k^{-2}$ [see *Chelton et al.*, 2006]. It is clear that the ECMWF wind field lacks power at all scales, but this is particularly clear at scales less than around 1000 km. Introducing the tip jet through the

**Table 2.** Wind Speed Statistics in the Box Given by 55–65 °N, 20–45 °W for QuikSCAT, ECMWF and ECMWF With Tip Jet Parameterization Over the 32 Test Cases[a]

| | ECMWF | ECMWF+TJ | QuikSCAT |
|---|---|---|---|
| Mean | 11.55 | 12.14 | 13.42 |
| Max. | 25.95 | 35.00 | 42.31 |
| Min. | 0.22 | 0.22 | 1.00 |
| SD | 4.8 | 5.5 | 5.47 |
| A | 13.00 | 13.71 | 15.12 |
| C | 2.58 | 2.32 | 2.62 |

[a]All values have units of m s$^{-1}$ other than the Weibull shape parameter, *C*, which is dimensionless.

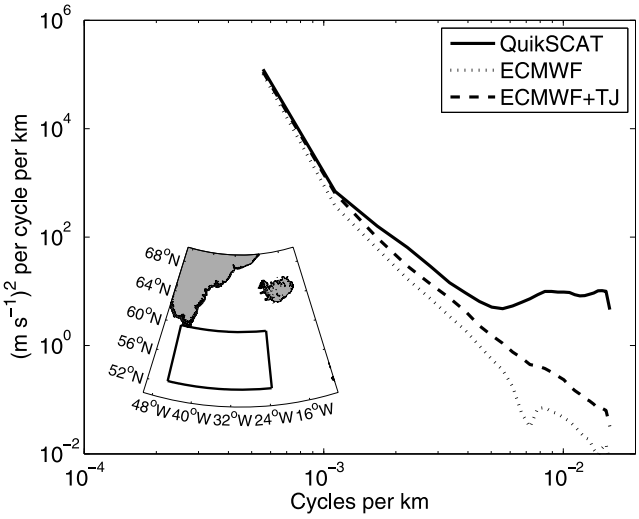


**Figure 12.** Power spectral density from the L3 gridded QuikSCAT data, ECMWF and ECMWF with the tip jet parameterization in the area 52–60 °N, 23.5–45.5 °W, estimated via Welch's method, for the 32 tip jet test cases. ECMWF data were first bi-linearly interpolated onto the QuikSCAT grid and the QuikSCAT data were slightly smoothed using a 5 point smoother. The graphic inset shows the area over which the spectra were calculated.

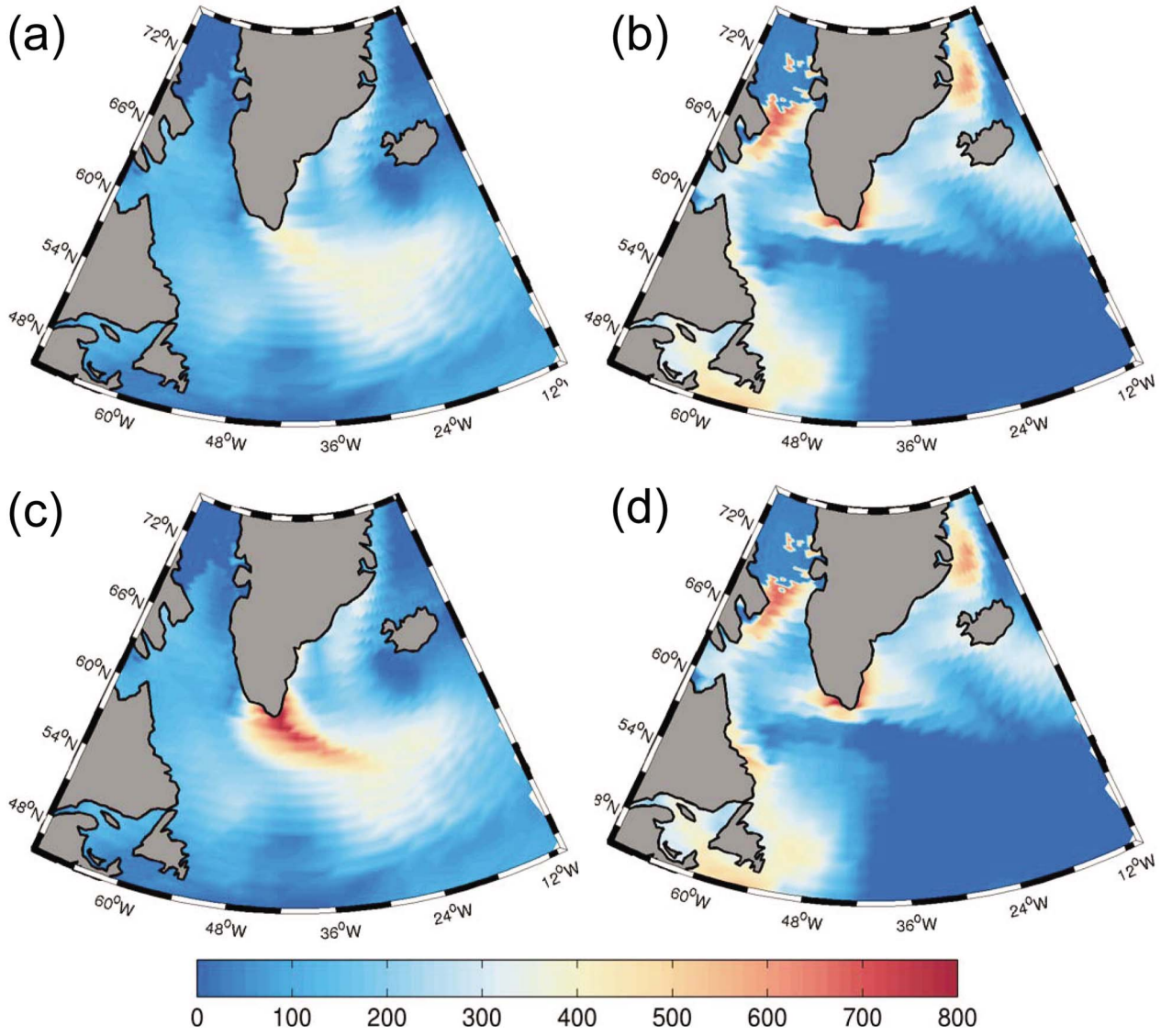


**Figure 13.** Total turbulent heat fluxes (W $m^{-2}$) in ERA-40 and ERA40+TJ for a typical (a, c) westerly (12Z, Oct. 25, 1981) and (b, d) easterly (12Z, Jan. 18, 1981) tip jet.

parameterization adds power at scales between 100 km and 1000 km, bringing the power spectral density closer to that of QuikSCAT.

## 6. Enhanced Surface Fluxes

### 6.1. Latent and Sensible Fluxes

[29] The heat fluxes in ERA-40 in a typical westerly tip jet case (Figure 13a) are elevated around the tip of Cape Farewell, with values of around 650 W $m^{-2}$. However, once the parameterized tip jet has been inserted (Figure 13b), the total turbulent heat fluxes in the core of the jet are increased to over 1200 W $m^{-2}$. These are even greater than the heat fluxes off the Labrador coast, which peak at around 1100 W $m^{-2}$. The causes of the strong fluxes in these two locations are somewhat different. Those in the Labrador Sea are caused by very cold, dry air being advected from the continent, while those in the tip jet are caused by stronger winds with a slightly smaller air/sea temperature difference. The sensible heat fluxes associated with the westerly tip jet seen here are consistent with those seen by *Doyle and Shapiro* [1999].

[30] During testing both with and without the parameterization over the winter (JFM) of 1980, the average combined sensible and latent heat flux over the southern Irminger Sea using the ERA-40 forcing was 123 W $m^{-2}$, with a maximum value of 846 W $m^{-2}$. Using the ERA40+TJ forcing, the average flux increased to 132 W $m^{-2}$, i.e. an increase of 9 W $m^{-2}$ on average. While this may seem to be a modest increase, one must bear in mind that we are averaging over an area much larger than an average sized tip jet. Averaging for this period over just those grid points which were perturbed by the parameterization gives values of 254 W $m^{-2}$ in ERA40+TJ, an increase of over 90 W $m^{-2}$ over ERA-40. Furthermore the maximum flux increased to 1492 W $m^{-2}$, suggesting that significant changes in forcing occur in the Irminger Sea.

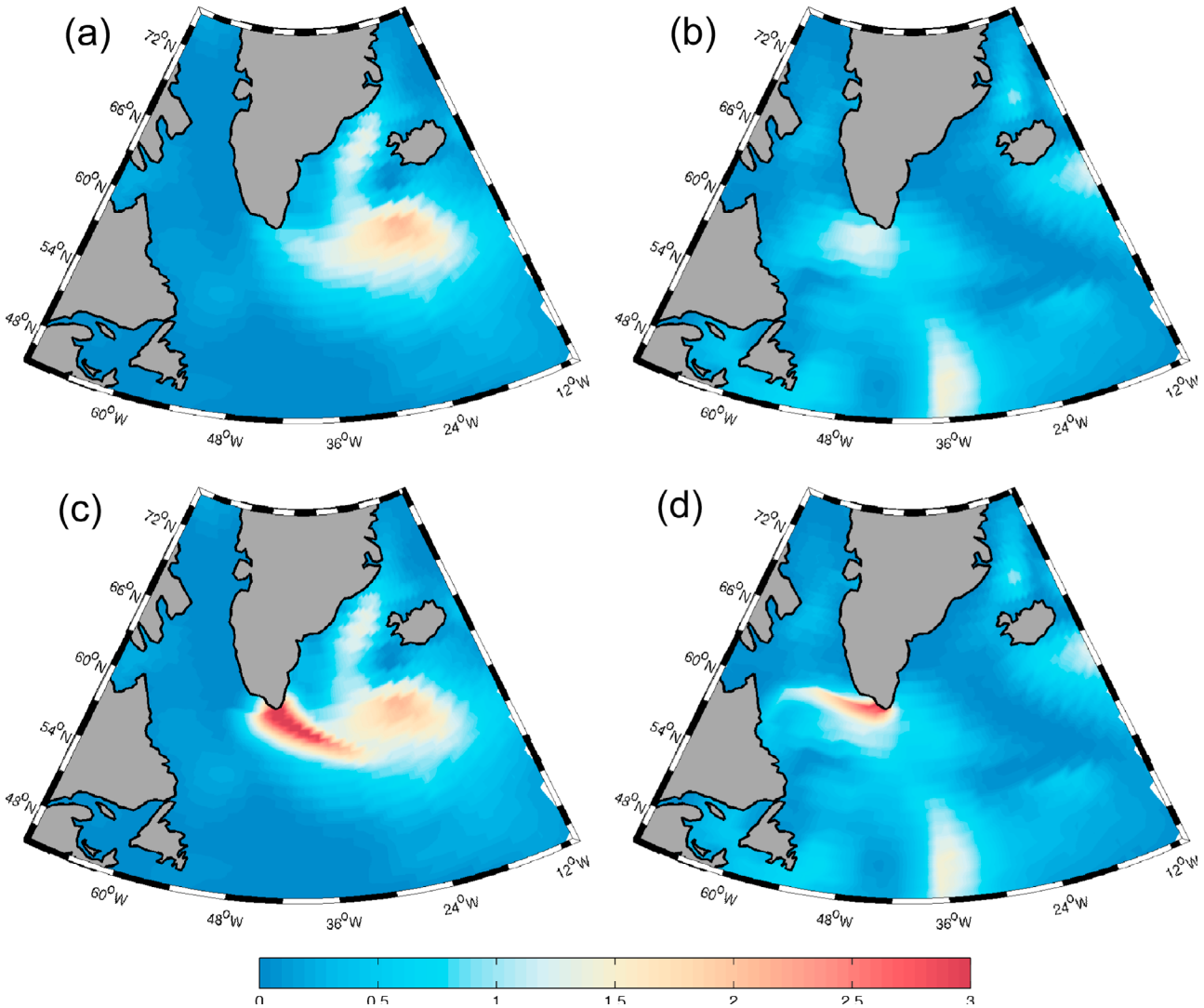


**Figure 14.** Momentum fluxes (N m$^{-2}$) in ERA-40 and ERA40+TJ for a typical (a, c) westerly (12Z, Oct. 25, 1981) and (b, d) easterly (12Z, Jan. 18, 1981) tip jet.

[31] In contrast to the westerly tip jet, the easterly tip jet has a relatively minor impact on heat fluxes. In the example shown in Figures 13c and 13d, heat fluxes are only increased in the region of the easterly tip jet by around 60 W m$^{-2}$. This is largely in agreement with *Sproson et al.* [2008], who used synoptic-scale arguments and float data to show that the easterly tip jet is not of comparable importance to the westerly jet in forcing open ocean convection. This is due to the fact that air in the easterly tip jet has become heavily modified, and is of a warm, moist, maritime nature. It should be noted, however, that *Martin and Moore* [2007] did see modestly enhanced heat fluxes of around 200 W m$^{-2}$ in the vicinity of a easterly tip jet. It seems, therefore, that conditions do arise in which the easterly jet can enhance air-sea heat exchange, although this is not generally the case.

[32] In January–February–March 1980, the average sensible plus latent heat flux over the south-east Labrador Sea was 187 W m$^{-2}$ with a maximum combined flux of 1116 W m$^{-2}$. Once the easterly tip jet had been bogussed into the wind field, the average combined flux showed a modest increase of 2 W m$^{-2}$, up to 189 W m$^{-2}$.

### 6.2. Momentum Fluxes

[33] Figure 14 shows the momentum fluxes associated with the same parameterized westerly tip jet and easterly tip jet cases as in Figure 13. The momentum flux calculated from the unperturbed wind field does show an enhanced transfer of momentum between the atmosphere and ocean, in the vicinity of the westerly and easterly tip jets. However, due to the under-representation of the jets, the peak momentum flux is only of the order of 1.5 N m$^{-2}$ for the westerly tip jet and 1 N m$^{-2}$ for the easterly jet. Once the tip jet and easterly tip jet have been bogussed into the wind field, these peak values rise to 3.5 N m$^{-2}$ for the westerly jet and 3 N m$^{-2}$ for the easterly jet. Note that in the westerly case, there is a further area of relatively strong wind stress, which is associated with a synoptic-scale cyclone to the south of Iceland. It is also important to note the strong meridional gradients in the wind stress, which will provide locally large magnitudes of wind stress curl. *Pickart et al.* [2003b] and *Spall and Pickart* [2003] note the importance of localized strong wind stress curl in forcing the oceanic circulation, both in the immediate vicinity

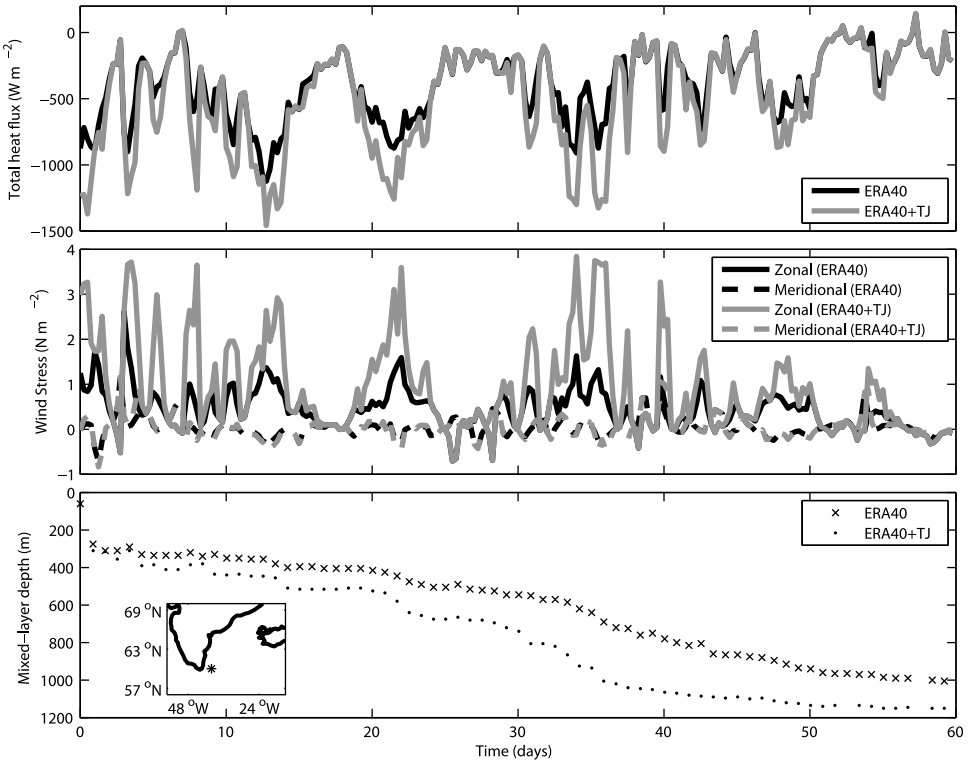


**Figure 15.** Mixed-layer development in the Irminger Sea in a 1-D model, using time series of heat and momentum flux both with and without the tip jet parameterization. The top panel shows the total heat flux applied to the model, the middle panel shows the surface meridional and zonal wind stress, and the bottom panel shows the development of the mixed-layer. The graphic inset shows the location from where the time series were extracted.

and elsewhere in the sub-polar gyre through the propagation of Rossby waves away from the source. For example, *Spall and Pickart* [2003] suggest that the Labrador Sea gyre is driven by localized wind stress curl east of Greenland, communicated by topographically steered Rossby waves.

## 7. Impact on a 1-D Ocean

[34] To provide a simple demonstration of the influence of the tip jet parameterization on the ocean, we turn to a one-dimensional mixed-layer ocean model [*Price et al.*, 1986], used previously in studies of the impact of Greenland tip jets on oceanic mixed-layer development [*Våge et al.*, 2008; *Sproson et al.*, 2008]. To initialize the model, temperature and salinity profiles were obtained from an Argo float in the Irminger Sea (59.3 °N, 37.7 °W) on December 29th, 2008. Forcing time series of total heat flux and wind stress were then extracted from the ERA-40 forcing fields for 60 days from 1st January, 1983, when the NAO was in a positive state (+1.8). Two runs were carried out, one using the standard ERA-40 forcing fields (control run), and one using the perturbed ERA40+TJ fields (perturbed run). In both runs, a vertical resolution of 5 m and temporal resolution of 60 s were used, with a background diffusion coefficient of $10^{-5}$ m$^2$ s$^{-1}$.

[35] Figure 15 (top) shows the total heat flux that would be extracted from the ocean. As expected, the heat fluxes are similar when they are small; where they differ the fluxes from the tip jet run are stronger as the increased wind is introduced into the forcing fields. The largest differences between the perturbed and control runs are approximately 500 W m$^{-2}$ around day 36 of the integration. Similar increases in the momentum flux are also seen (Figure 15, middle), although these are relatively larger, as $\tau \propto U^2$. The largest increases in momentum flux again occur around day 36, and are greater than 2 N m$^{-2}$. The zonality of the tip jet is maintained in the parameterization, with nearly all of the momentum increase in the zonal direction. Depending on the orientation of the tip jet, increases can also be seen in the meridional component (for example there is an increase of around 0.5 N m$^{-2}$ in the meridional wind stress component at day 40). Figure 15 (bottom) shows the ocean mixed-layer development for each of the forcing time series. The pattern of deepening is similar in both of the runs, but the run with the perturbed time series deepens more during each high-flux event. The largest difference between the two runs occurs around day 36, with the perturbed run around 300 m deeper than the control. After this, the mixed-layer in the perturbed run encounters a layer of increased stratification. As there are no further robust tip jet events, the difference between the two runs decreases, resulting in a difference in mixed-layer depth of 170 m at the end of the 60 day integration. Although there are no validation data for this particular model run, previous studies [e.g., *Våge et al.*, 2008] have indicated that inclusion of the tip jet improves the evolution of the mixed-layer depth in the Irminger Sea as compared with observations, and by a comparable amount to the differences seen here.

## 8. Conclusions

[36] We have developed a method for bogussing both westerly and easterly Greenland tip jets into a wind field. The parameterization development has made use of a data set of 32 westerly and 42 easterly tip jets, but can be implemented without recourse to this data set. The method allows for the variation of strength, shape, size and orientation that are observed in tip jets and thus accurately reproduces a tip jet, allowing it to be smoothly blended into the background field. The westerly tip jet can cause a significant, if localized, increase in sensible and latent heat flux which we have demonstrated has a significant impact on ocean mixed-layer depth and thus potentially on convection in ocean models. The effect of the easterly jet is more modest. This is in agreement with previous work [*Sproson et al.*, 2008], which suggests that the easterly tip jet is not of great importance in forcing open ocean convection. Both the westerly and easterly tip jets cause a large local increase in wind stress, and their relatively small meridional scale leads periodically to strong dipoles of wind stress curl, which have previously been linked to circulation patterns in the North Atlantic.

[37] The parameterization does not rely on any external data sets, only mean sea level pressure and surface wind fields, and can thus be easily implemented into either ocean only general circulation models or coupled climate models at the coupling stage, once consideration has been given to the transfer of heat between the ocean and atmosphere.

[38] A future paper will examine the impact of both westerly and easterly tip jets on local and global ocean circulation, by implementing the parameterization into a global ocean general circulation model and examining 'control' and 'perturbation' experiments.

[39] **Acknowledgments.** We thank two anonymous reviewers for their insightful comments which have helped to greatly improve this work. Data have been provided by ECMWF (www.ecmwf.int), Coriolis Data Center (www.coriolis.eu.org) and the Physical Oceanography DAAC (podaac.jpl.nasa.gov). This study was funded as part of a NERC studentship, grant NER/S/A/2006/14110.

## References

Bakalian, F., S. Hameed, and R. Pickart (2007), Influence of the Icelandic low latitude on the frequency of Greenland tip jet events: Implications for Irminger Sea convection, *J. Geophys. Res.*, *112*, C04020, doi:10.1029/2006JC003807.

Chelton, D. B., M. H. Freilich, J. M. Sienkiewicz, and J. M. Von Ahn (2006), On the use of QuikSCAT scatterometer measurements of surface winds for marine weather prediction, *Mon. Weather. Rev.*, *134*, 2055–2071.

Condron, A., G. R. Bigg, and I. A. Renfrew (2008), Modeling the impact of polar mesocyclones on ocean circulation, *J. Geophys. Res.*, *113*, C10005, doi:10.1029/2007JC004599.

Doyle, J. D., and M. A. Shapiro (1999), Flow response to large-scale topography: The Greenland tip jet, *Tellus, Ser. A*, *51*, 728–748.

Ebuchi, N., H. C. Graber, and M. J. Caruso (2002), Evaluation of wind vectors observed by QuikSCAT/SeaWinds using ocean buoy data, *J. Atmos. Oceanic Technol.*, *19*, 2049–2062.

Hu, A., and G. A. Meehl (2009), Effect of the Atlantic hurricanes on the oceanic meridional overturning circulation and heat transport, *Geophys. Res. Lett.*, *36*, L03702, doi:10.1029/2008GL036680.

Lavender, K. L., R. E. Davis, and W. B. Owens (2000), Mid-depth recirculation observed in the interior Labrador and Irminger seas by direct velocity measurements, *Nature*, *407*, 66–69.

Marshall, J., and F. Schott (1999), Open ocean deep convection: Observations, models and theory, *Rev. Geophys.*, *37*, 1–64.

Martin, R., and G. W. K. Moore (2007), Air-sea interaction associated with a Greenland reverse tip jet, *Geophys. Res. Lett.*, *34*, L24802, doi:10.1029/2007GL031093.

Mesinger, F., et al. (2006), North American regional reanalysis, *Bull. Am. Meteorol. Soc.*, *87*, 343–360.

Moore, G. W. K. (2003), Gale force winds over the Irminger Sea to the east of Cape Farewell, Greenland, *Geophys. Res. Lett.*, *30*(17), 1894, doi:10.1029/2003GL018012.

Moore, G. W. K., and I. A. Renfrew (2005), Tip jets and barrier winds: A QuikSCAT climatology of high wind speed events around Greenland, *J. Clim.*, *18*, 3713–3725.

Nansen, F. (1912), Das Bodenwasser und die Abkühlung des Meeres, *Int. Rev. Gesamten Hydrobiol. Hydrogr.*, *5*, 1–42.

Outten, S. D., I. A. Renfrew, and G. N. Petersen (2009), An easterly tip jet off Cape Farewell, Greenland. II: Simulations and dynamics, *Q. J. R. Meteorol. Soc.*, *135*, 1934–1949. (Correction, *Q. J. R. Meteorol. Soc.*, *136*, 1099, 2010.)

Pavia, E. G., and J. J. O'Brien (1986), Weibull statistics of wind speed over the ocean, *J. Clim. Appl. Meteorol.*, *25*, 1324–1332.

Pickart, R. S., D. J. Torres, and R. A. Clarke (2002), Hydrography of the Labrador Sea during active convection, *J. Phys. Oceanogr.*, *32*, 428–457.

Pickart, R. S., F. Straneo, and G. W. K. Moore (2003a), Is Labrador Sea water formed in the Irminger basin?, *Deep Sea Res., Part I*, *50*, 23–52.

Pickart, R. S., M. A. Spall, M. H. Ribergaard, G. W. K. Moore, and R. F. Milliff (2003b), Deep convection in the Irminger Sea forced by the Greenland tip jet, *Nature*, *424*, 152–156.

Price, J. F., R. A. Weller, and R. Pinkel (1986), Diurnal cycling: Observations and models of the upper ocean response to diurnal heating, cooling, and wind mixing, *J. Geophys. Res.*, *91*, 8411–8427.

Renfrew, I. A., G. W. K. Moore, P. S. Guest, and K. Bumke (2002), A comparison of surface layer and surface turbulent flux observations over the Labrador Sea with ECMWF analyses and NCEP reanalyses, *J. Phys. Oceanogr.*, *32*, 383–400.

Renfrew, I. A., et al. (2008), The Greenland Flow Distortion Experiment, *Bull. Am. Meteorol. Soc.*, *89*, 1307–1324.

Renfrew, I. A., G. N. Petersen, D. A. J. Sproson, G. W. K. Moore, H. Adiwidjaja, S. Zhang, and R. North (2009a), A comparison of aircraft-based surface-layer observations over Denmark Strait and the Irminger Sea with meteorological analyses and QuikSCAT winds, *Q. J. R. Meteorol. Soc.*, *135*, 2046–2066.

Renfrew, I. A., S. D. Outten, and G. W. K. Moore (2009b), An easterly tip jet off Cape Farewell, Greenland. Part I: Aircraft observations, *Q. J. R. Meteorol. Soc.*, *135*, 1919–1933.

Spall, M. A., and R. S. Pickart (2003), Wind-driven recirculations and exchange in the Labrador and Irminger seas, *J. Phys. Oceanogr.*, *33*, 1829–1845.

Sproson, D. A. J., I. A. Renfrew, and K. J. Heywood (2008), Atmospheric conditions associated with oceanic convection in the south-east Labrador Sea, *Geophys. Res. Lett.*, *35*, L06601, doi:10.1029/2007GL032971.

Talley, L. D., and M. S. McCartney (1982), Distribution and circulation of Labrador Sea water, *J. Phys. Oceanogr.*, *12*, 1189–1205.

Våge, K., R. S. Pickart, G. W. K. Moore, and M. H. Ribergaard (2008), Winter mixed-layer development in the central Irminger Sea: The effect of strong, intermittent wind events, *J. Phys. Oceanogr.*, *38*, 541–565.

Våge, K., R. S. Pickart, T. Spengler, H. C. Davis, and R. S. Pickart (2009), Multi-event analysis of the Greenland tip jet based upon 45 winters in ERA-40, *Q. J. R. Meteorol. Soc.*, *135*, 1999–2011.

Wüst, G. (1935), Schichtung und Zirkulation des Atlantischen Ozeans: Die Stratosphäre, *Wiss. Ergeb. Dtsch. Atl. Exped.*, *6*, 109–288.

K. J. Heywood, I. A. Renfrew, and D. A. J. Sproson, School of Environmental Sciences, University of East Anglia, Norwich NR4 7TJ, UK. (d.sproson@uea.ac.uk)